Supporting Information

Ling et al. 10.1073/pnas.1200109109

SI Results and Discussion

Crystallization and Structure Determination. Crystals of MST1 were obtained by sitting drop vapor-diffusion method. Equal volumes of the protein solution (6–8 mg/mL) and the well buffer were mixed, and the drops were incubated at 12 °C for 2–4 wk. The high-resolution crystal form of apo MST1 was obtained from 0.1 M Hepes, pH 7.5 and 2 M ammonium sulfate, whereas the low-resolution crystal form grew in the presence of 0.2 M magnesium formate and 20% PEG 3,350. The crystals containing the MST1-TAM binary complex were grown when a mixture of MST1, $tRNA_2^{Thr}$, 1 mM $MgCl_2$, and 1 mM threonyl sulfamoyl adenylate was incubated over 0.1 M cacodylate, pH 6.5, 2 M ammonium sulfate, and 0.2 M NaCl. All crystals were cryoprotected either with 3.2 M ammonium sulfate or 20% glycerol prior to X-ray exposure. Data were collected at liquid nitrogen temperature at Southeast Regional Collaborative Access Team 22-ID and 22-BM beamlines at the Advanced Photon Source, Argonne National Laboratory. The diffraction data were processed in HKL2000 (1). The crystal structure of apo MST1 was determined by molecular replacement in Phaser (2) using the *Escherichia coli* and *Staphylococcus aureus* ThrRS (PDB ID codes 1QF6 and 1NYR) as search models. The refined apo MST1 was used to phase other MST1 crystal forms. The structure refinement was performed in Phenix (3), and the model building was done in Coot (4, 5). All figures were produced in PyMOL (The PyMOL Molecular Graphics System, Version 1.2, Schrödinger, LLC).

Conformational Flexibility of the Aminoacylation Domain in apo MST1. In addition to structures described in the main text, we have determined a crystal structure of apo MST1 derived from the orthorhombic crystal form, which contained two MST1 dimers in the asymmetric unit and that diffracted X-rays to 3.5-Å resolution (Fig. S4 and Table S1). Although the overall structure is very similar to the one derived from the tetragonal crystal form (rmsd of 0.74 Å), several major structural differences in the conformation of the aminoacylation domain were observed. In particular, the β-sheet that forms the floor of the active-site groove and helix α7, which is connected to strands β9 and β10 of that β-sheet, rotated approximately 14° clockwise around the vertical axis when the molecule is viewed in the orientation shown in the central panel of Fig. S4. Moreover, helix α4, strands β5 and β6, and the β5–β6 loop undergo a conformational change as well. As already discussed in the main text, these particular elements sit atop the active site and form a lid that might regulate the access of the substrate to the active site. The extent of the conformational change is identical to the one observed in the crystal structure of the MST1-TAM binary complex. This suggests that the binding of TAM does not promote this particular conformational change but rather stabilizes the "open" conformation of this segment of the catalytic domain. Based on our structural results, we propose that the lid of the active-site groove in MST1 exists in the equilibrium between the closed and open conformation. The open conformer presumably has higher affinity for L-threonine, ATP, and threonyl-AMP. On substrate binding, the open conformation of the lid is stabilized and the ligand is locked in the active-site groove. Likewise, the conformational movements in the central β-sheet and helix α7 of the catalytic domain might resemble the putative conformational change the enzyme might undergo on binding the acceptor arm of $tRNA^{Thr}$. Future studies on MST1-tRNA binary complexes will shed more light on these aspects of MST1 structure.

1. Otwinowski Z, Minor W (1997) Processing of X-ray diffraction data collected in oscillation mode. *Methods Enzymol* 276:307–326.
2. McCoy AJ, et al. (2007) Phaser crystallographic software. *J Appl Crystallogr* 40:658–674.
3. Adams PD, et al. (2010) PHENIX: A comprehensive Python-based system for macromolecular structure solution. *Acta Crystallogr D Biol Crystallogr* 66:213–221.
4. Emsley P, Cowtan K (2004) Coot: Model-building tools for molecular graphics. *Acta Crystallogr D Biol Crystallogr* 60:2126–2132.
5. Krissinel E, Henrick K (2004) Secondary-structure matching (SSM), a new tool for fast protein structure alignment in three dimensions. *Acta Crystallogr D Biol Crystallogr* 60:2256–2268.

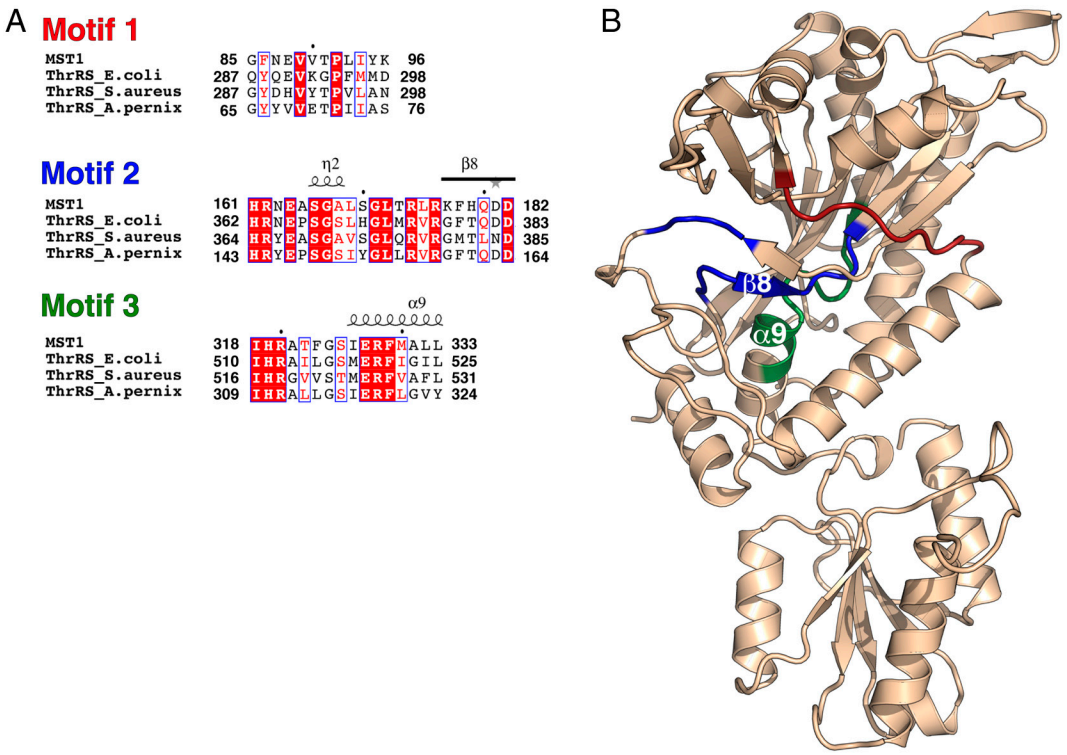

Fig. S1. The signature motifs of class II aaRS are present in MST1. (*A*) Excerpts of a sequence alignment between MST1 and *Escherichia coli*, *Staphylococcus aureus*, and *Aeropyrum pernix* threonyl-tRNA synthetase (ThrRS). Only the segments spanning the conserved signature motifs are shown. (*B*) The signature motifs are highlighted on the ribbon diagram of apo MST1 (beige). The view is rotated 90° anticlockwise relative to the Fig. 1*A*, *Left*. Motif 1 is red, motif 2 is blue, and motif 3 is green.

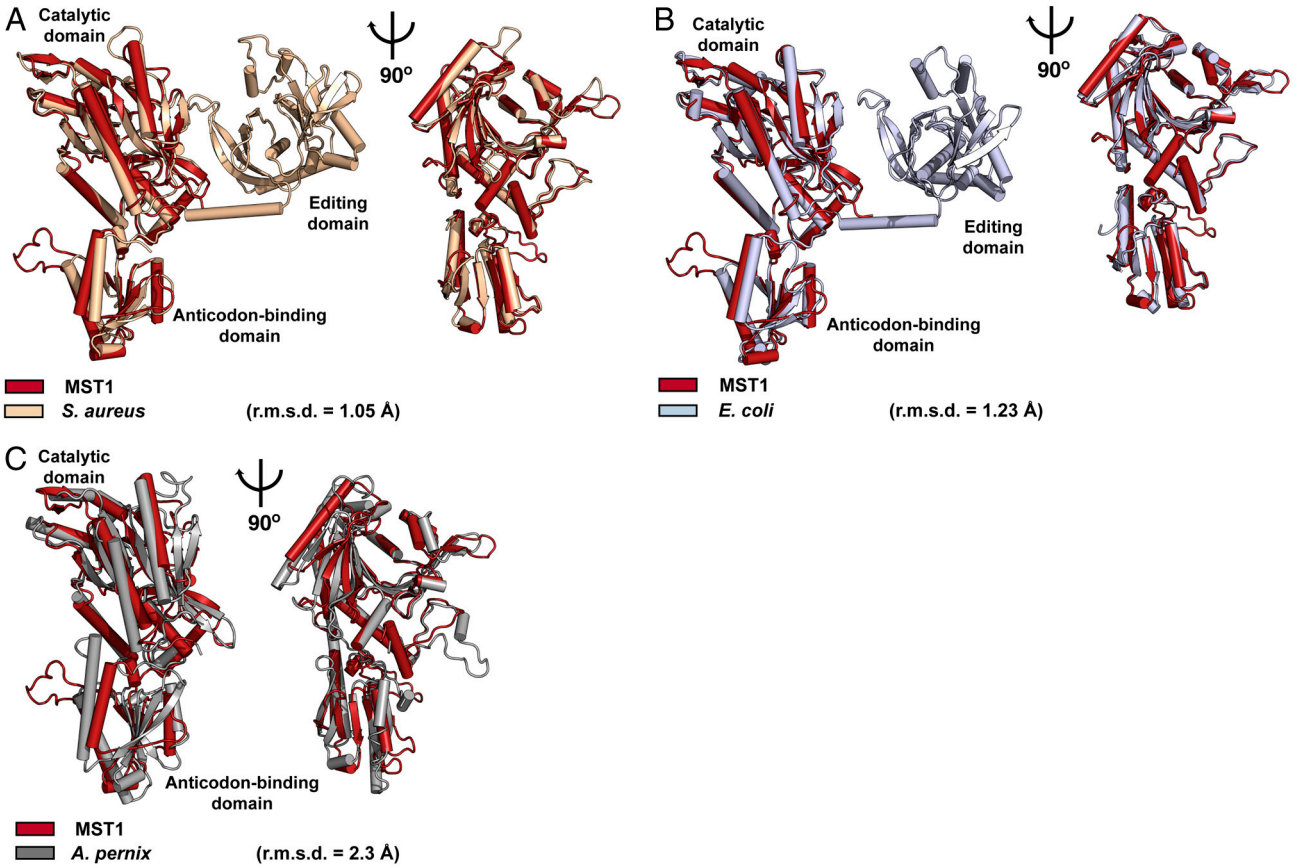

Fig. S2. Structural comparison reveals that MST1 is closely related to bacterial and distinct from the archaeal ThrRSs. (*A*) Superpositioning of the catalytic and anticodon-binding domains of *S. aureus* ThrRS (beige) onto that of MST1 (red) reveals that these two enzymes have similar three-dimensional architecture. (A) The left-hand side clearly shows that MST1 lacks a large N-terminal editing domain present in all bacterial ThrRSs. The right-hand side is rotated approximately 90° clockwise and is oriented to look down the active-site crevice. The editing domain of *S. aureus* ThrRS is removed for clarity. (*B*) The same analysis as in *A*, but using the *E. coli* ThrRS (light blue). (*C*) The structural comparison with *A. pernix* ThrRS (gray) reveals significant differences between the yeast mitochondrial and archaeal enzymes in spite of the fact that both enzymes lack the *cis*-editing domain.

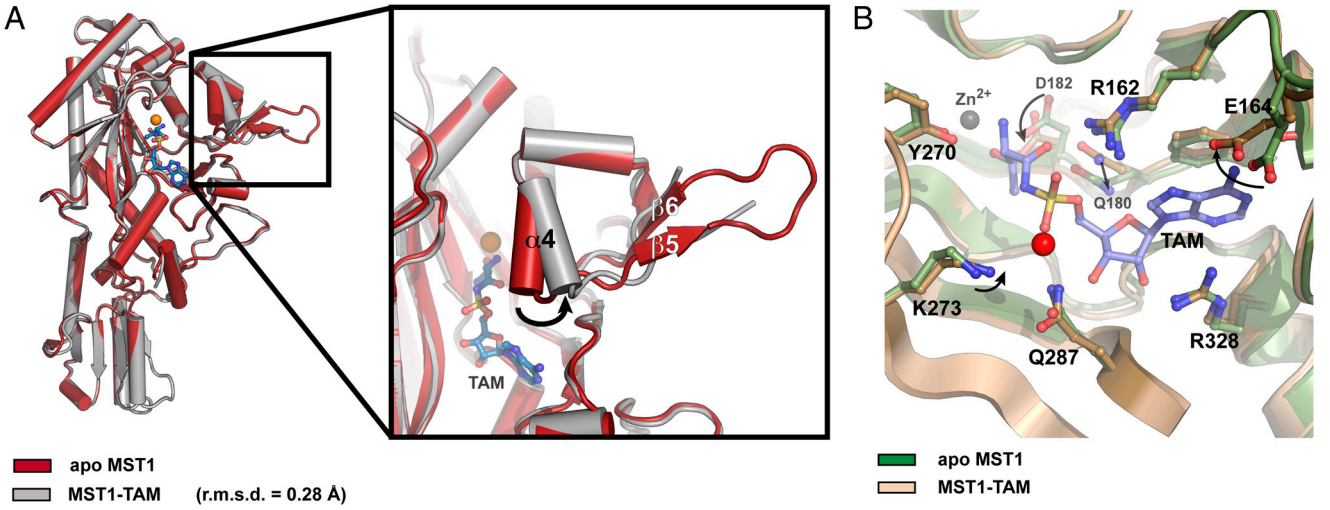

Fig. S3. Binding of threonyl-adenylate stabilizes the open conformation of MST1. (*A*) Superpositioning of apo MST1 (red) onto the binary MST1-TAM complex (gray) reveals a conformational change in helix α4 and strands β5 and β6 on analog binding. This change is emphasized in the area delineated with a black box. The β5–6 loop is disordered in the crystal of the binary complex. TAM is shown as blue balls-and-sticks, and Zn^{2+} is orange. (*B*) TAM binding induces subtle conformational rearrangements in the active-site of MST1. The apo MST1 structure (green) is superimposed onto the MST1-TAM binary complex structure (beige). The major movements of the active-site residues are shown with arrows. TAM is shown as blue balls-and-sticks, the hydrolytic water is a red sphere, and Zn^{2+} is gray.

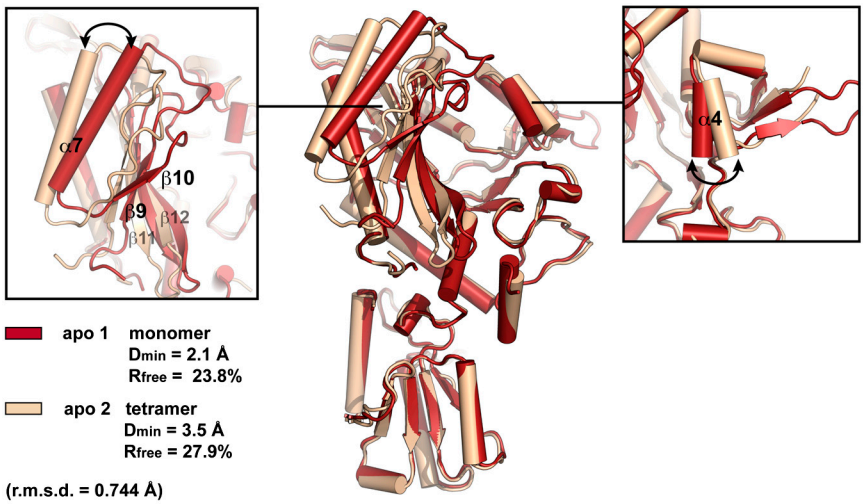

Fig. S4. The catalytic domain of apo MST1 adopts distinct conformations. (*Center*) A comparison between the apo-MST1 structures derived from two crystal forms reveals that the catalytic domain of MST1 can sample different conformations. (*Left*) The largest movement is observed in the β-sheet that forms the floor of the active-site crevice. Also, helix α7, which is linked to strands β9 and β10, undergoes a significant rotation (shown with arrow). (*Right*) Helix α4, strands β5 and β6, and the loop β5–β6 adopt different conformations as well. This conformational change is similar to the one observed on binding of the threonyl-adenylate analog to MST1, which suggests that the apo-catalytic domain samples the "closed" and "open" conformations and that analog binding stabilizes the open conformation. The ribbon diagrams representing the high- and low-resolution apo-MST1 are red and beige, respectively.

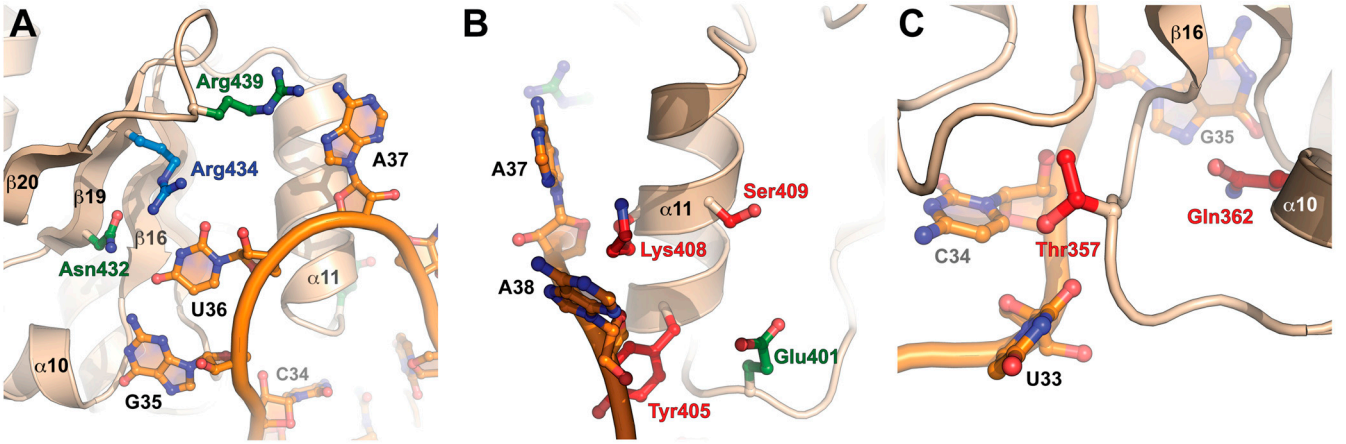

Fig. S5. Distinct structural elements in MST1 and their possible role in $tRNA^{Thr}$ recognition. (*A*) Strand β19 is important for $tRNA_1^{Thr}$ recognition as well as for binding to both of the $tRNA^{Thr}$ species. For instance, Arg434 presumably recognizes the distinct conformation of the backbone or it interacts with one of the bases in the enlarged anticodon loop of $tRNA_1^{Thr}$. On the other hand, Asn432 and Arg439 perhaps establish similar interactions with both $tRNA_1^{Thr}$ and $tRNA_2^{Thr}$. (*B*) Tyr405, Lys408, and Ser409 in helix α11 might interact with the backbone or specific base in $tRNA_2^{Thr}$. In contrast, Glu401 is likely to play a similar role in binding to both $tRNA^{Thr}$ species. (*C*) The β16–α10 loop is another structural element that distinguishes two tRNAs. The side chains of Thr357 and Gln362 are likely to interact with the 5′ end of the anticodon loop of $tRNA_2^{Thr}$ but not with that of $tRNA_1^{Thr}$.

Table S1. Data collection and refinement statistics

Crystal	apo MST1 #1	apo MST1 #2	MST1-TAM
Space group	P 4_3 2_1 2	C 2 2 2_1	P 4_3 2_1 2
Cell dimensions, Å	$a = b = 68$, $c = 191$	$a = 154$, $b = 158$, $c = 237$	$a = b = 68.5$, $c = 192.3$
Data collection			
Resolution limit, Å	2.1	3.6	2.0
Unique reflections	26,825	33,252	29,684
Completeness (overall/last shell), %	98.6/87.0	97.5/83.8	93.4/99.9
R_{sym} (overall/last shell), %	10.7/41.2	16.2/80.2	10.1/37.3
$I/\sigma I$ (overall/last shell)	26/3.7	10.7/1.7	21.6/8.6
Redundancy (overall/last shell)	28.4/6.0	6.4/4.8	11.0/11.7
Refinement			
Average B-factor, Å^2			
Protein	30.1	90.2	27.8
Ions, ligands. solvent	34.8	64.5	34.4
Number of atoms (protein)	3,498	13,409	3,448
Number of atoms (ions, ligand)	35	4	36
Number of solvent molecules	310	46	318
R_{work} $(\|F\| > 0\sigma)$, %	20.5	23.7	20.1
R_{free} $(\|F\| > 0\sigma)$, %	25.0	27.5	25.6
Rms deviations from ideality			
Bond lengths, Å	0.005	0.005	0.004
Bond angles, °	0.882	0.729	0.908